25. Manning, A. M., Williams, A. C., Gamie, S. M. & Paraskeva, C. *Oncogene* **6,** 1471–1476 (1991).
26. Rodeck, U. *et al. Cancer Res.* **54,** 575–581 (1994).
27. Hannon, G. J., Demetrick, D. & Beach, D. & Beach, D. *Genes Dev.* **7,** 2378–2391 (1993).
28. Xiong, Y. *et al. Nature* **366,** 701–704 (1993).

ACKNOWLEDGEMENTS. We thank S. Matsumoto and C. Gawel for technical assistance and P. Renna, M. Ockler and J. Duffy for photography and graphics. M. Stampfer (Berkeley), M. Meyerson (MGH), P. Boukamp and N. Fusenig (German Cancer Research Center) provided critical reagents. We are grateful to Hui Zhang for providing baculoviral lysates and for helpful discussions. G.J.H. is a fellow of the Damon Runyon–Walter Winchell Cancer Research Fund. D.B. is an Investigator of the Howard Hughes Medical Institute. This work was supported in part by the NIH.

Location of a folding protein and shape changes in GroEL–GroES complexes imaged by cryo-electron microscopy

Shaoxia Chen*, Alan M. Roseman*, Allison S. Hunter*, Stephen P. Wood*, Steven G. Burston†, Neil A. Ranson†, Anthony R. Clarke† & Helen R. Saibil*

* Department of Crystallography, Birkbeck College London, London WC1E 7HX, UK
† Department of Biochemistry and Centre for Molecular Recognition, University of Bristol, Bristol BS8 1TD, UK

PROTEIN folding mediated by the molecular chaperone GroEL occurs by its binding to non-native polypeptide substrates and is driven by ATP hydrolysis[1]. Both of these processes are influenced by the reversible association of the co-protein, GroES (refs 2–4). GroEL and other chaperonin 60 molecules[5] are large, cylindrical oligomers consisting of two stacked heptameric rings of subunits[6,7]; each ring forms a cage-like structure[8] thought to bind polypeptides in a central cavity[8–10]. Chaperonins play a passive role in folding by binding or sequestering folding proteins to prevent their aggregation[11–13], but they may also actively unfold substrate proteins trapped in misfolded forms, enabling them to assume productive folding conformations[14–16]. Biochemical studies show that GroES improves the efficiency of GroEL function[2,3,17], but the structural basis for this is unknown. Here we report the first direct visualization, by cryo-electron microscopy, of a non-native protein substrate (malate dehydrogenase) bound to the mobile, outer domains at one end of GroEL. Addition of GroES to GroEL in the presence of ATP causes a dramatic hinge opening of about 60°. GroES binds to the equivalent surface of the GroEL outer domains, but on the opposite end of the GroEL oligomer to the protein substrate.

Size-exclusion chromatography of purified GroEL in the presence of ATP releases a significant amount of residually bound protein and peptide to generate an 'emptied' state. Cryo-electron microscope (cryo-EM) side- and end-view projections (Figs 1 and 2*a*, *b*) of this emptied GroEL were aligned and averaged, and a three-dimensional reconstruction was calculated from the averages by backprojecting the seven symmetry-related side views and the end view. Figure 1*c* shows a central section (21 Å thick) of this map. The side projection shows that the overall dimensions of the 14-mer are 140 Å high by 130 Å wide. The end projection is not 7-fold averaged, and demonstrates the strong 7-fold symmetry of the structure. The side-view section (Fig. 2*c*) shows the two major domains of each subunit, with the inner domains forming the interface between top and bottom heptameric rings, and outer domains surrounding a 35–40-Å diameter hole. A three-dimensional surface-contoured view of the structure is shown in Fig. 4*b*.

The stable complex between GroEL and malate dehydrogenase (MDH) was formed by mixing GroEL with a 2.4-fold molar excess of chemically denatured MDH (GroEL 14-mer : MDH monomer) to saturate the available binding sites (see Fig. 2 legend). Figure 2*d–f* shows the cryo-EM images of this binary complex. Comparison with the 'empty' structure reveals a distinct region of additional density at only one end of the oligomer in the side views, and extra density fills the hole seen in the end projection. Difference maps of the end projection and the section are shown in Fig. 2*g* and *h* with the empty GroEL contours superimposed. These maps locate the MDH density in one end cavity of GroEL, between the outer domains and protruding slightly. The visible ligand density (which has been rotationally averaged about the vertical axis in the section view; Fig. 2*h*) occupies a volume roughly similar to that of the 34,000-M_r native subunit (approximately $50 \times 30 \times 35$ Å), but diffuse density may extend into a larger volume. The asymmetric complex is consistent with a spectroscopically determined binding stoichiometry of 1:1 (refs 18, 19, and S.G.B. and A.R.C., unpublished observations), and implies negative cooperativity of ligand binding.

Binding of Mg–ATP to GroEL is sufficient to release some substrate proteins, but others are not released into productive folding forms by ATP unless GroES is also present. To investigate the structural influence of Mg–ATP alone, a set of cryo-EM images of empty GroEL incubated in Mg–ATP were collected and are shown in Fig. 3*a–c*. Compared with GroEL (Fig. 2*c*), GroEL–ATP shows a slight vertical expansion of the oligomer (from 140 to 150 Å) owing to an opening of the outer domains (Fig. 3*a*, *c*). This outer domain displacement differs from that deduced from previous negative stain electron microscopic work[8]. An important factor seems to be the presence of tightly bound substrates in the earlier study, as cryo-EM images of the GroEL–ATP complex made from non-emptied GroEL more closely resemble the previous negative stain findings (not shown). On the basis of the present cryo-EM data, there may be a slight asymmetry in the GroEL–ATP complex. The three-dimensional view of GroEL–ATP in Fig. 4*c* shows the petal-like opening of the outer domains.

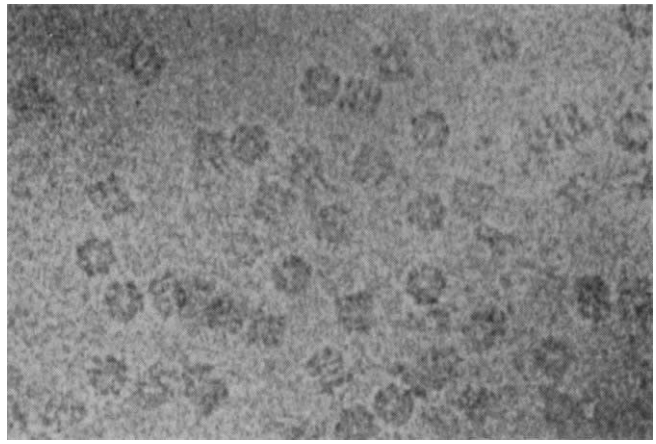

200 Å

FIG. 1 Unstained, frozen-hydrated GroEL oligomers were imaged in vitreous ice over holes in the carbon support film. The dark regions represent protein density, contrasted against the background of vitreous ice. Two orientations of the oligomers are present: end views, which show the 7-fold symmetry, and side views with four layers of density. METHODS. Solutions containing 1–2 mg ml^{-1} GroEL in 10 mM ammonium acetate and 10 mM Tris buffer pH 7.6 were prepared at room temperature, vitrified by plunging into liquid ethane and imaged at −170 °C. Cryo-EM was done on a JEOL 1200 EX microscope with an Oxford Instruments cryotransfer stage. All images used in the following analysis were recorded with an electron dose ≈10 e Å^{-2} and with a defocus in the range 500–850 nm.

The vertical expansion of GroEL induced by nucleotide binding is greatly enhanced in the presence of GroES. In the conditions used here, the great majority of complexes formed between GroEL and GroES in the presence of ATP are asymmetrical, with GroES bound to one end of GroEL (Fig. 3*d–f*). The interaction with GroES traps the adjacent GroEL outer domains in a wide-open conformation (Fig. 3*f*). Estimating orientations by taking lines along the direction of elongation of the density, we find that the angle between inner and outer domains increases by as much as 60°. A smaller domain movement brought about by a 5–10° rotation of the hinge occurs on binding ATP alone (Fig. 3*c*), and also in the ring not bound to GroES in the complex (Fig. 3*f*, bottom). An enclosed, dome-shaped volume of maximum height 65 Å and maximum width 80 Å is formed by GroES binding and the hinge opening. A surface-contoured view of the three-dimensional map of the complex is shown in Fig. 4*d*.

When the stable GroEL–MDH complex is combined with GroES and ATP, MDH folding is initiated (N. Dunster and A.R.C., unpublished results). To determine the relationship between GroES and substrate-binding sites, we trapped this folding complex by vitrification 15 s after adding GroES and ATP (Fig. 3*g–i*). The MDH density occurs at the opposite end of GroEL to GroES, between the free outer domains, which are slightly farther apart, as in the ATP form. A similar ternary complex is seen with ADP as the nucleotide (not shown). Note that after 15 s approximately half the initially bound ATP would have been hydrolysed[14,20].

Figure 4*a* is a diagram representing the subunit outlines of the chaperonin complexes. The ends of the GroEL outer domains provide the binding sites for the protein substrate, and these surfaces are pushed apart on binding ATP as a consequence of the rotation about the inter-domain hinge. When ATP is present, GroES binds to the equivalent surface on the widely opened outer domains, creating the enclosed cavity in the GroEL–GroES complex. In the ternary complex, substrate is not seen in the GroES-enclosed cavity, but is found in the binding cavity on the opposite ring.

There is also evidence for substrate binding to the side of GroEL opposite GroES by antibody labelling[21], but a cross-

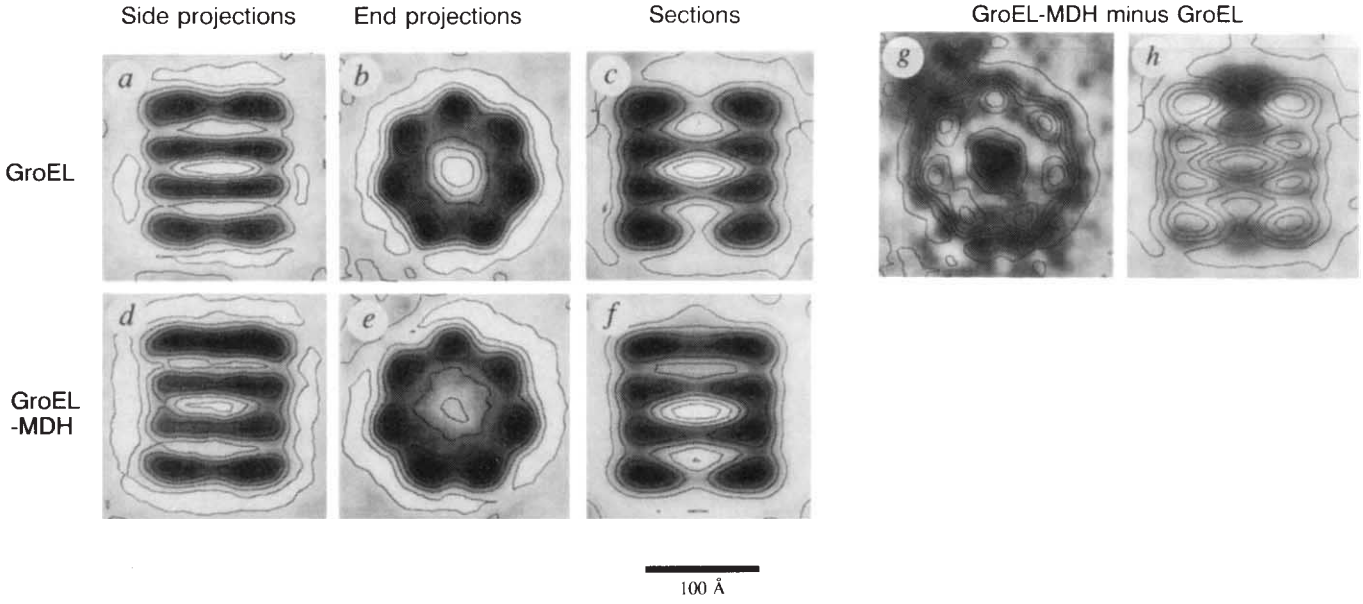

FIG. 2 *a*, An averaged side-view projection of 418 individual images aligned by correlation methods, showing the typical four-layered density. *b*, End-view projection, average of 490 molecules, showing the 7-fold symmetry. *c*, A 21-Å-thick section through the 3-D map generated from *a* and *b*, showing four subunits in vertical section. The connecting bridges between the domains and also the subunit contacts between rings are near the outer surface of the cylinder. *d–f*, The corresponding views of the GroEL–MDH complex. The side projection (*d*, average of 368 views) and section *f* show additional density at one end of the oligomer, and the end projection (*e*, average of 329 views) shows the extra density in the central hole. *g*, *h*, Difference maps of GroEL–MDH minus GroEL, showing the distribution of MDH density in the complex. The differences are shown as grey-scale density, with the contours of empty GroEL superimposed for reference. The darkest regions show the location of MDH density in the binary complex. *g*, End-view difference map, showing the MDH density in the central hole in projection. No symmetry averaging was applied to this view. *h*, Section difference map, showing the location of rotationally averaged MDH between the outer domains of GroEL and protruding slightly from the GroEL surface. The vertical position of MDH is not affected by the symmetry averaging.

METHODS. *Escherichia coli* GroEL and GroES were prepared as described[27]. To discharge residual bound polypeptide, GroEL was applied to a Sepharose 4-B chromatography column (100 cm × 2.6 cm) in 2 mM ATP in 20 mM $MgCl_2$, 50 mM KCl, 50 mM triethanolamine-HCl, pH 7.5. The GroEL–MDH complex was prepared by rapidly injecting 200 µl of 1.2 µM GroEL (14-mer) onto a 2.8-µl drop of 200 µM porcine mitochondrial MDH (subunits) in 3 M guanidinium chloride. Circular dichroism spectra showed complete loss of MDH secondary structure at 2 M guanidinium chloride. Saturation of MDH binding at 1:1 stoichiometry was confirmed by two methods, that is, suppression of recovery of enzyme activity and titration of binding of pyrene-labelled, unfolded MDH to GroEL. Micrographs were recorded at ×30,000 on Agfa EM film and digitized with a CCD camera at a final resolution of 5.6 Å per pixel. Particle alignment was done by iterative cross-correlation, using procedures written for SPIDER and SEMPER software systems. Averages of manually aligned views for each sample provided initial templates for cross-correlation. To assess the resolution, the raw images forming each average were split to form two half-averages, and phase residuals were determined by comparing the two halves, showing that the information was significant to ~25 Å. Three-dimensional reconstructions calculated by back-projection from symmetry-related, averaged views had sufficient angular resolution (indicating preferential orientation about the 7-fold axis parallel to the air–water interface) to align them with the corresponding end projections. Inclusion of the end views in the reconstructions improved the angular resolution but had little effect on the appearance of the 21-Å-thick section views. Surface-contoured representations of the 3-D maps are shown in Fig. 4*b–d*.

linking study implies substrate binding adjacent to GroES[22]. The 'same-side' complex may be present transiently, as GroES is bound and released during cycles of ATP binding and hydrolysis[2], and GroES can bind to both ends simultaneously[20,23–25]. However, the double-sided complex is not symmetrical, as the second GroES binds more weakly and the nucleotide state may differ at the two ends[20]. Given that the substrate can remain bound to the ATP ternary complex for ⩾15 s and if the GroES–GroEL–GroES complex occurs as an intermediate, there remains the possibility of a transient state in which GroES encapsulates the substrate. However, we have no evidence for occupation of a GroES-capped cavity, and, furthermore, our results cast doubt on the recent proposal that substrate proteins bind to the exterior of the GroEL cylinder[26].

This work gives the first direct image of a chaperone-bound, folding protein and allows visualization of dramatic structural

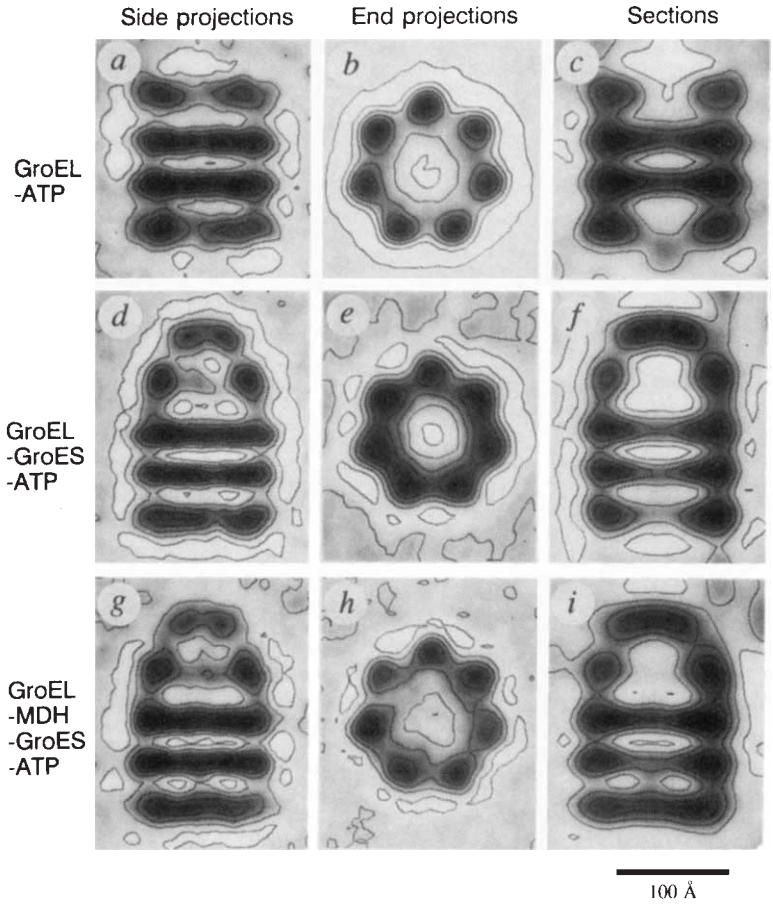

FIG. 3 Cryo-electron microscopy of GroEL–ATP (*a–c*), GroEL–GroES–ATP complexes (*d–f*) and GroEL–GroES–ATP–MDH complexes (*g–i*). *a*, Side projection average of 186 views of GroEL–ATP. The overall size of the oligomer is 150 × 130 Å. *b*, End projection average of 496 views. *c*, Section of the 3-D map generated from *a* and *b*, as in Fig. 1, showing the enlarged gap between the outer domains. *d*, Side projection average of 245 views, showing GroES binding to one end of GroEL, which is in a more open configuration. *e*, End projection average of 252 views, showing the 7-fold symmetry. *f*, Section of 3-D map generated from *d* and *e*, showing the large hinge opening between GroEL subunit domains in the ring binding GroES, and the internal cavity formed by GroES capping the opened-up structure. *g*, Side projection average of 328 views of the GroEL–MDH–GroES–ATP ternary complex, showing additional density in the ring opposite GroES. *h*, Average of 243 end views of the ternary complex. *i*, Section of the 3-D map generated from *g* and *h*, showing MDH density in the lower ring.
METHODS. The GroEL–ATP and GroEL–GroES–ATP complex were formed by mixing 1.2 μM GroEL (14-mer) with 2 mM ATP in the standard buffer, with or without 3.6 μM GroES (7-mer). The ternary complex was formed by adding GroES and ATP to the GroEL–MDH complex formed as described in Fig. 2 legend. The GroEL–GroES complexes were frozen 15–30 s after mixing, GroEL–ATP samples were frozen after 10–20 min of incubation in Mg–ATP, and the ternary complex samples were frozen 15 s after adding GroES and ATP. Addition of 40 mM guanidinium chloride alone had no effect on the appearance of the GroEL–GroES–ATP complex, and very similar ternary complexes were obtained with acid- and urea-denatured MDH (not shown).

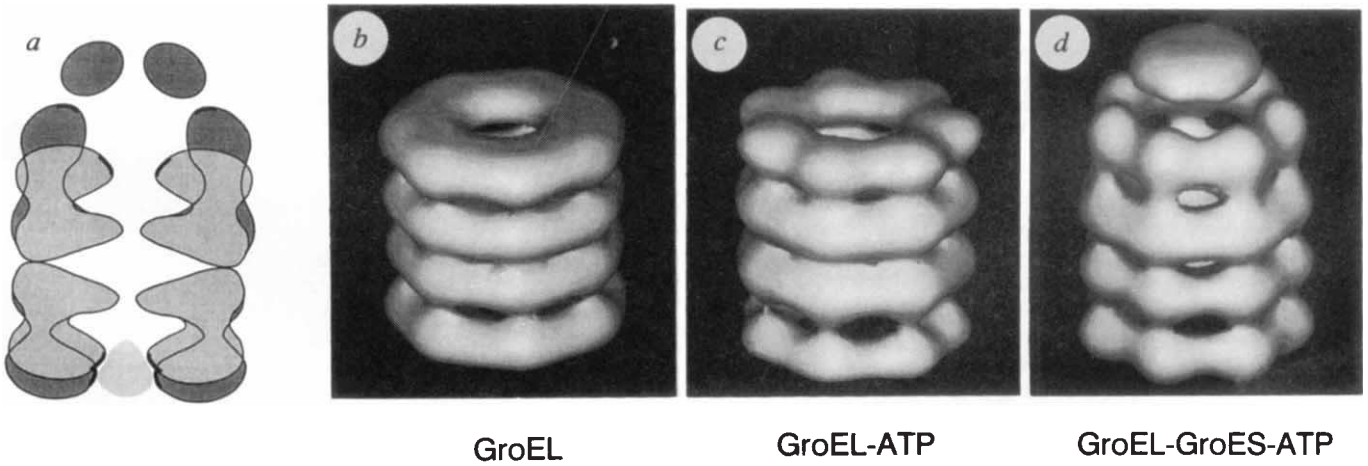

FIG. 4 *a*, Diagram derived from the outer contours of empty GroEL and GroEL–GroES sections, showing the dramatic reorientation of the outer domains of GroEL in contact with GroES. The ligand position is shown as a shaded area to illustrate the point that the end of the outer domain, which binds substrate, rotates out to interact with GroES. The interaction site is indicated by a darker line. *b*, The external shape of GroEL seen in a surface-rendered view of the 3-D reconstruction as a solid, reflective object slightly tipped towards the viewer. *c*, 3-D reconstruction of GroEL–ATP, showing the opening of the outer domains widening the substrate-binding cavity. *d*, The same representation of the GroEL–GroES–ATP complex, showing the pronounced vertical expansion of GroEL, the location of GroES as a disk above GroEL, and the enlargement of the cavity. 3-D surface rendering was done on the University of London Computer Centre Convex using the program AVS.

changes associated with ATP and GroES binding. GroEL provides binding surfaces for substrate proteins on a ring of highly mobile domains. □

Received 20 May; accepted 24 August 1994.

1. Hendrick, J. P. & Hartl, F. U. *A. Rev. Biochem.* **62,** 349–384 (1993).
2. Martin, J., Mayhew, M., Langer, T. & Hartl, F. U. *Nature* **366,** 228–233 (1993).
3. Fisher, M. *J. biol. Chem.* **269,** 13629–13636 (1994).
4. Schmidt, M., Buchner, J., Todd, M. J., Lorimer, G. H. & Viitanen, P. V. *J. biol. Chem.* **267,** 10304–10311 (1994).
5. Kubota, H., Hynes, G., Carne, A., Ashworth, A. & Willison, K. *Curr. Biol.* **4** 89–99 (1994).
6. Hendrix, R. W. *J. molec. Biol.* **129,** 375–392 (1979).
7. Hutchinson, E. G., Tichelaar, W., Hofhaus, G., Weiss, H. & Leonard, K. *EMBO J.* **8,** 1485–1490 (1989).
8. Saibil, H. R. *et al. Curr. Biol.* **3,** 265–273 (1993).
9. Langer, T., Pfeifer, G., Martin, J., Baumeister, W. & Hartl, F. U. *EMBO J.* **11,** 4757–4765 (1992).
10. Braig, K., Simon, M., Furuya, F., Hainfeld, J. F. & Horwich, A. L. *Proc. natn. Acad. Sci. U.S.A.* **90,** 3978–3982 (1993).
11. Ellis, R. J. & Hemmingsen, S. M. *Trends biochem. Sci.* **14,** 339–342 (1989).
12. Goloubinoff, P., Christeller, J. T., Gatenby, A. A. & Lorimer, G. H. *Nature* **342,** 884–889 (1989).
13. Nilsson, B. & Anderson, S. *A. Rev. Microbiol.* **45,** 607–635 (1991).
14. Jackson, G. S. *et al. Biochemistry* **32,** 2554–2563 (1993).
15. Zahn, R., Spitzfaden, C., Ottiger, M., Wüthrich, K. & Plückthun, A. *Nature* **368,** 261–265 (1994).
16. Peralta, D., Hartman, D. J., Hoogenraad, N. J. & Høj, P. B. *FEBS Lett.* **339,** 40–45 (1994).
17. Martin, J. *et al. Nature* **352,** 36–42 (1991).
18. Mendoza, J. A., Lorimer, G. H. & Horowitz, P. M. *J. biol. Chem.* **266,** 16973–16976 (1991).
19. Badcoe, I. G. *et al. Biochemistry* **30,** 9195–9200 (1991).
20. Todd, M. J., Viitanen, P. V. & Lorimer, G. H. *Science* **265,** 659–666 (1994).
21. Ishii, N., Taguchi, H., Sasabe, H. & Yoshida, M. *J. molec. Biol.* **236,** 691–696 (1994).
22. Bochkareva, E. S. & Girshovich, A. S. *J. biol. Chem.* **267,** 25672–25675 (1992).
23. Harris, J. R., Plückthun, A. & Zahn, R. *J. struct. Biol.* (in the press).
24. Llorca, O., Marco, S., Carrascosa, J. L. & Valpuesta, J. M. *FEBS Lett.* **345,** 181–186 (1994).
25. Schmidt, R. *et al. Science* **265,** 656–659 (1994).
26. Azem, A., Kessel, M. & Goloubinoff, P. *Science* **265,** 653–656 (1994).
27. Staniforth, R. A. *et al. FEBS Lett.* **344,** 129–135 (1994).

ACKNOWLEDGEMENTS. We thank J. Munn for EM support, R. Westlake and J. Bouquiere for computing support, R. J. Ellis and G. Laxer for discussion, the Birkbeck Photo Unit for photographic work and the Wellcome Trust and AFRC for project grants. A.R.C. is a Lister Institute Fellow.

TABLE 1 Parameters of β-sheet formation

Amino acid	ΔΔG (kcal mol^{-1})	T_m (°C)	$K_a/K_a^{AAA\text{-}44Thr}$	ΔΔΔG (kcal mol^{-1})
Thr	0.83	60.2	1.0	−0.27
Ser	0.63	59.4	3.1	−0.07
Glu	0.31	57.0	1.5	0.30
Val	0.17	56.1	1.5	−0.65
Phe	0.16	56.1	1.1	−0.70
Tyr	0.11	55.9	1.1	−0.75
Cys	0.08	55.1	0.7	−0.44
Gln	0.04	54.7	1.9	−0.19
Ile	0.02	54.8	1.6	−0.98
Ala	0	54.7	2.9	0
His	−0.01	54.6	1.8	0.01
Met	−0.02	54.2	1.8	−0.74
Asp	−0.10	53.7	1.2	0.84
Trp	−0.17	53.3	3.0	−0.77
Asn	−0.24	52.6	1.0	−0.16
Leu	−0.24	52.8	1.0	−0.75
Lys	−0.40	51.4	0.9	−0.67
Arg	−0.43	51.2	1.0	−0.88
Gly	−0.85	47.6	1.4	0.35
Pro	< −4	<0	0	—

Listed are ΔΔG values for β-sheet formation at an edge position relative to alanine, thermal melting temperatures (T_m) for the AAA-44Xaa proteins, relative binding constants (K_a) to human Fc for the AAA-44Xaa proteins, and ΔΔΔG values for β-sheet formation, comparing $\Delta\Delta G_{edge} - \Delta\Delta G_{centre}$ values (see also ref. 2). The K_a for wild-type GB1 is 1.4×10^8 M^{-1} (ref. 30). The $K_a/K_a^{AAA\text{-}44Thr}$ value for wild-type GB1 is 7.1. ΔG values for unfolding at 321 K were calculated as described previously[2] using data obtained from CD thermal unfolding measurements and the Gibbs-Helmholz equation. A positive ΔΔG value indicates an increase in stability relative to alanine. Estimated errors in determination of T_m and ΔG are ±0.5 °C and ±0.06 kcal mol^{-1} respectively. Fc binding was measured as described previously[2] by adding variable amounts of competitor protein to a fixed quantity of protein G-alkaline phosphatase at 5 °C in 96-well plates. The ratio of affinity constants for the mutants was normalized to AAA-44Thr. GB1-Thr1 (see Fig. 1 legend) was included as an internal standard on each plate.

Context is a major determinant of β-sheet propensity

Daniel L. Minor Jr* & Peter S. Kim†

Departments of * Chemistry and † Biology, Howard Hughes Medical Institute, Whitehead Institute for Biomedical Research, Massachusetts Institute of Technology, Nine Cambridge Center, Cambridge, Massachusetts 02142, USA

RESIDUES in β-sheets occur in two distinct tertiary contexts: central strands, bordered on both sides by other β-strands, and edge strands, bordered on only a single side by another β-strand[1]. The ΔΔG values for β-sheet formation measured at an edge β-strand of the IgG-binding domain of protein G(GB1) are quite different from those obtained previously[2,3] at a central position in the same protein. In particular, there is no correlation at the edge position with statistically determined β-sheet-forming preferences[4]. The differences between β-sheet propensities measured at central and edge β-strands, ΔΔΔG values, correlate with the values of water/octanol transfer free energies[5] and side-chain non-polar surface area for the amino acids[6]. These results strongly suggest that, unlike α-helix formation, β-sheet formation is determined in large part by tertiary context, even at solvent-accessible sites, and not by intrinsic secondary structure preferences.

The 20 naturally occurring amino acids were substituted at a solvent-exposed edge β-strand position, residue 44, by site-directed mutagenesis in a host molecule in which local interactions to the guest site had been minimized by replacing the nearest neighbours with alanine (see Fig. 1 legend). This edge β-strand is bordered on one side by another β-strand and on the other side by solvent (Fig. 1*a*). The stability of each protein (denoted AAA-44Xaa) was measured by thermal unfolding as monitored by circular dichroism (CD) at 218 nm (Fig. 1*b*). ΔΔG values for β-sheet formation, referenced to alanine, were obtained by assuming that changes in global stability result entirely from changes in the ability of the residue at the guest site to adopt a β-sheet conformation. In support of this assumption, molecules representative of the entire ΔΔG range were found to have $\Delta H_{van't\ Hoff}/\Delta H_{cal}$ ratios near unity, indicating that the two-state nature of the equilibrium unfolding transition observed for wild-type GB1 (ref. 7) remains intact (see Fig. 1 legend). The relative free energy differences for β-sheet formation at the edge position are listed in Table 1.

All the proteins tested, with the exception of unfolded AAA-44Pro, bind Fc with around sevenfold reduced affinity relative to wild-type GB1 (Table 1). There is some variation in binding constants but this is not correlated with protein stability. As residues 42–46 have been identified as participants in the Fc-binding interface[8,9] it seems likely that the observed affinity differences reflect direct effects on binding by substitutions at residue 44.

As a more detailed check on the conformation at the guest site of each molecule, the chemical shifts of the aromatic ring protons of Trp 43 were measured in each of the 20 variants. Trp 43 is expected to be sensitive to changes in structure as it immediately precedes the guest site and is part of the hydrophobic core of the molecule. The chemical shifts of the Trp 43 ring protons are similar in all the variants, with the exception